Simultaneous and Continuous Estimation of Joint Angles Based on Surface Electromyography State-Space Model

Xugang Xi, Wenjun Jiang, Xian Hua, Huijiao Wang, Chen Yang, Yun-Bo Zhao, *Senior Member, IEEE*, Seyed M. Miran, and Zhizeng Luo

***Abstract*—Simultaneous and continuous joint angle estimation plays an important role in motion intention recognition and rehabilitation training. A surface electromyography (sEMG) state-space model is proposed to estimate simultaneous and continuous lower-limb-joint movements from sEMG signals in this article. The model combines the forward dynamics with Hill-based muscle model (HMM), making the extended model capable of estimating the lower-limb-joint motion directly. sEMG features including root-mean-square and wavelet coefficients are then extracted to construct a measurement equation used to reduce system error and external disturbances. With the proposed model, unscented Kalman filter is used to estimate joint angle from sEMG signals. In the experiments, sEMG signals were recorded from ten subjects during muscle contraction involving three lower-limb-joint motions (knee-joint motion, ankle-joint motion, and simultaneous knee-ankle-joint motion). Comprehensive experiments are conducted on three motions and the results show that the mean root–mean–square error for knee-joint motion, ankle-joint motion, and simultaneous motion of the proposed model are 5.1143°, 5.2647°, and 6.3941°, respectively, and significant improvements are demonstrated compared with the traditional methods.**

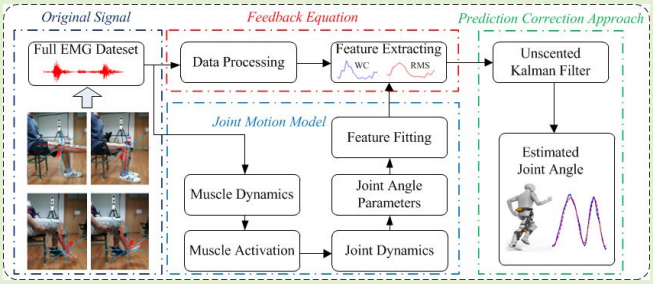

***Index Terms*— Surface electromyography (sEMG), muscle model, feature extraction, continuous joint motion.**

I. Introduction

IN HUMAN-MACHINE interaction (HMI), surface electromyography (sEMG) is an ideal signal source for controlling robot or intelligent limb through human motion intention, because it is easy to be recorded and contains sufficient human body's movement information [1]–[4]. Discrete action control is a common way to control artificial limbs, typically including 4–10 fixed hand movements or hand gesture (clench the hand, stretch the palm, etc.) [5]. Zhang *et al.* [6] proposed a framework based on accelerometer and sEMG sensors to distinguish 18 kinds of hand gestures, and achieved high recognition rate. Discrete action control based on sEMG is a simple and robust control method. But it can only predict discrete limb actions and cannot recognize the continuous variable (e.g., angle and acceleration in continuous joint motion) and simultaneous joint motion. Therefore, the robot and artificial limb controlled by discrete action cannot complete the simultaneous multi-joint motions continuously and smoothly. However, forecasting the continuous motion variables is the key to achieve smooth control of the intelligent limb [7], [8] in the field of rehabilitation medical robots.

Currently, many achievements have already been made in estimating continuous joint movement. Chen *et al.* [9] used Multi-Feature Fusion with Random Forest (RF) to estimate the ankle joint angles, compared to BP neural network algorithms, the training speed of RF was far faster, while the accuracy of the estimation was similar. Chen *et al.* [10] proposed a simple-structure temporal information-based model to estimate

Manuscript received November 8, 2020; accepted December 25, 2020. Date of publication January 4, 2021; date of current version February 17, 2021. This work was supported in part by the National Natural Science Foundation of China under Grant 61971169, Grant 61673350, and Grant 60903084; in part by the Zhejiang Provincial Key Research and Development Program of China under Grant 2021C03031; and in part by the Jinhua Science and Technology Bureau under Grant 2019-3-020. The associate editor coordinating the review of this article and approving it for publication was Prof. Kea-Tiong Tang. *(Corresponding author: Xugang Xi.)*

Xugang Xi, Wenjun Jiang, Chen Yang, and Zhizeng Luo are with the School of Automation, Hangzhou Dianzi University, Hangzhou 310018, China, and also with the Key Laboratory of Brain Machine Collaborative Intelligence of Zhejiang Province, Hangzhou 310018, China (e-mail: xixi@hdu.edu.cn; 1301931380@qq.com; 171060060@hdu.edu.cn; luo@hdu.edu.cn).

Xian Hua is with the Jinhua People's Hospital, Jinhua 321000, China (e-mail: huaxiang1206@126.com).

Huijiao Wang is with the Hangzhou Vocational and Technical College, Hangzhou 310018, China, and also with the School of Automation, Hangzhou Dianzi University, Hangzhou 310018, China (e-mail: hjwang@hdu.edu.cn).

Yun-Bo Zhao is with the Department of Automation, Zhejiang University of Technology, Hangzhou 310023, China (e-mail: ybzhao@ieee.org).

Seyed M. Miran is with the Biomedical Informatics Center, George Washington University, Washington, DC 20052 USA (e-mail: miran@gwu.edu).

Digital Object Identifier 10.1109/JSEN.2020.3048983

upper limb motion, the results showed that the estimation accuracy of the model was better than the multilayer perception model. Li *et al.* [11] utilized sEMG signals to calculate the endpoint stiffness of human arm, and manipulate the robot arm. Xiao *et al.* [12] proposed a grey features weighted support vector machine (GFWSVM) to estimate elbow joint angle, and the result showed that the proposed algorithm had the better performance compared to BP, the radial basis function (RBF) and scaled conjugate gradient (SCG) neural network. They are based on data-driven algorithms. Some researchers explored the possibility of building the continuous estimation of joint angles from musculoskeletal models based on EMG [13]–[15]. The control strategy based on the physiological muscle model is that by simulating the control of human muscles, it may better mimic movement of human limb joint than data-driven algorithms, thus may obtain higher estimation accuracy.

Hill-based muscle model (HMM) is the one of physiological muscle model estimating continuous joint motion. A sEMG-based forward dynamics model which consists of HMM, muscle activation dynamics, and joint forward dynamics was proposed in [16]. This model involves many physiological parameters and is hard to calculate, thus limiting its practical applications. On this basis, Fleischer and Hommel [17] developed a simplified model for controlling extremity exoskeleton and then constructed a calibration process to optimize the estimation, which made some physiological parameters of model easy calculate. HMM is the most frequently used muscle model to estimates continuous joint motion, which however faces two challenges. First, HMM involves many complex physiological parameters. These parameters are difficult to identify and computationally heavy, making simplified models a favorite alternative. However, it introduces errors and degrades the estimation accuracy. Second, HMM is often used to calculate the joint torque directly from sEMG signals [18]. For continuous estimations of joint motion, the motion states (e.g. angular velocity and angle) are calculated from the sEMG-recognized torque indirectly. Thereby it brings accumulated errors and worsens the estimation accuracy.

To address the above challenges, this study developed a new model that fuses the HMM and the joint forward dynamics which can estimate the simultaneous and continuous multi-joint motion. The new model can calculate the joint motion from sEMG signals directly. Two sEMG features, RMS and wavelet coefficients (WC), are proposed to build the measurement equations. Then, a sEMG state-space model is created to estimate knee-joint angle, ankle-joint angle, and simultaneous knee-ankle-joint angle.

II. Materials and Methods

A. Data Acquisition

In the process of rehabilitation training, the flexion-extension of knee-joint and ankle-joint are common rehabilitation exercises. Fig. 1 illustrates the experimental setup. sEMG signals were measured from biceps femoris (BF), quadriceps femoris (QF), vastus lateralis (VL), vastus medialis (VM), gracilis (GR), tibialis anterior (TA), and gastrocnemius (GA), which are muscles relevant to lower limb motions. The experiment was carried out in 2 sections: with load 3kg

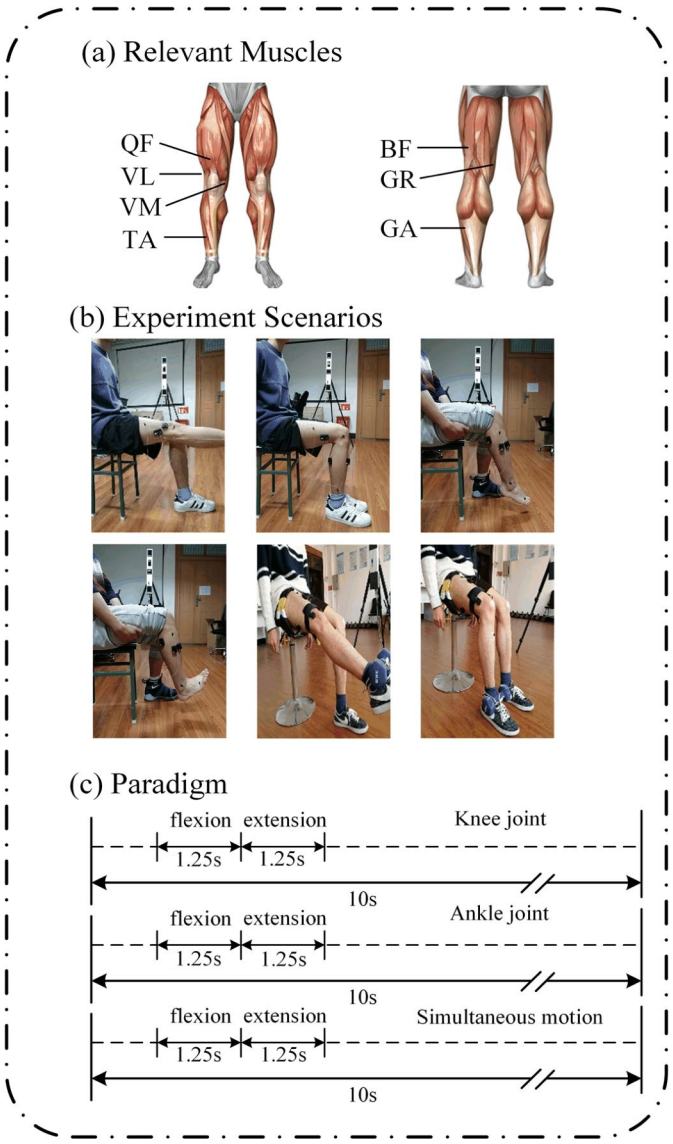

Fig. 1. Selection of relevant muscles and movement specification. (a) Relevant muscles in the experiments. (b) Movements in real-world scenes. (c) Time specification for the movements.

(The 3kg dumbbell is tied to the ankle of subject) and without load. In each section, subjects completed two types of joint motion alternately, which were knee joint flexion-extension, ankle joint flexion-extension and simultaneous motion of knee joint and ankle joint.

Trigno™Wireless EMG (Delsys Inc, Natick, MA, USA) was used to record sEMG signals. It provided 8-channel sEMG acquisition, a 16-bit resolution, a bandwidth of 20–450 Hz, and a baseline noise less than 1.25 μV. In the experiments, the sEMG signals were sampled at 2000 Hz. Codamotion (Charnwood Dynamics Limited, UK) was used to measure real-time joint-angle information. It is a piece of motion capture and analysis equipment which can obtain movement information of the object with active infrared.

Ten healthy subjects (five males and five females, 23±2 years old, weighing 50–70 kg) were tested in the experiments. All the subjects read and signed an informed

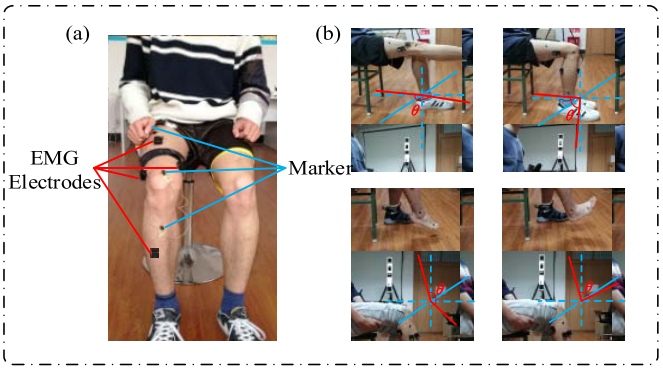

Fig. 2. (a) sEMG sensors arrangement. (b) experiment scenarios: knee joint flexion-extension motion and ankle joint flexion-extension motion.

consent form approved by an institutional review board. As shown in Fig. 2, sEMG signals were measured by surface electrodes. Each subject completed the action of knee joint flexion-extension, ankle joint flexion-extension, and simultaneous motion in 10s, and repeated four times with and without the load (3kg), respectively. The subjects were given an appropriate rest time after each trial to reduce muscle fatigue.

B. Data Preprocessing

sEMG signals are very weak, nonstationary, and random, and its effective frequency is 10-500Hz. Noise during the acquisition process of sEMG, 1) electronic equipment inherent noise, whose frequency ranges within zero to thousands of hertz. 2) environmental noise, it is mainly due to the capacitive coupling of the instrumentation and of the subject with power supply and the main frequency is 50Hz. 3) motion artifact caused by the relative movement of the surface of sensor and the skin in the experiment. To eliminate the inherent noise and motion artifacts, a bandpass filter (20-450Hz) was selected in the experiment.

The sampling frequency of joint-angle is much lower than that of sEMG, 100Hz for the former compared to 2000 Hz for the latter. To keep sEMG signals consistent with joint-angle signals, the features of every 20 data sequences of raw sEMG were extracted. After that, the subsampling frequency of sEMG signals was changed from 2000Hz to 100Hz.

C. sEMG State-Space Model

1) Hill-Based Muscle Model: The muscle activation model transforms sEMG signal to muscle activation. The neural activation was calculated from preprocessed sEMG signal through a recursive filter [19]. The muscle activation $a(k)$ can be described as follows [20],

$$a(k) = \frac{e^{A\cdot u(k)} - 1}{e^{A} - 1} \tag{1}$$

where $u(k)$ is the neural activation, k is the time, A is a nonlinear shape factor which can define the curvature.

Fig. 3 illustrates a simplified HMM. The HMM consists of a contractile element which produces the active muscle force

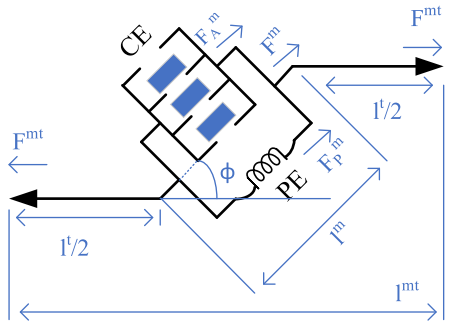

Fig. 3. Hill-based muscle model.

F_A^m and a parallel elastic element which produces the passive force F_P^m. The model can be described as follows:

$$F^m = F_P^m + F_A^m \tag{2}$$

The passive muscle force F_P^m is described as follows:

$$F_P^m = f_P(l) \cdot F_0^m, \quad l = l^m / l_0^m \tag{3}$$

where $f_P(l)$ is the normalized passive force-length relationship, F_0^m is the maximum isometric force, l is the normalized fiber length, l^m is the fiber length, and l_0^m is the optimal fiber length.

The active muscle force F_A^m is described as follows,

$$F_A^m = f_A(l) \cdot f_V(v) \cdot a(k) \cdot F_0^m, \quad v = v^m / v_0^m \tag{4}$$

where $f_A(l)$ is the normalized active force-length relationship, $f_V(v)$ is the normalized force-velocity relationship, v is the normalized fiber velocity, v^m is the contraction velocity, and v_0^m is the maximum of contraction velocity.

According to the equations above, the musculotendon force can be described as follows:

$$F^{mt} = [f_A(l) \cdot f_V(v) \cdot a(k) + f_P(l)] \cdot F_0^m \cdot \cos(\phi) \tag{5}$$

where F^{mt} is the musculotendon force, ϕ is the pennation angle.

The following simplifications can replace the biomechanical parameters [21], [22]:

$$\begin{aligned} f_A(l) &= \begin{cases} q_0 + q_1 \cdot l + q_2 \cdot l^2, & 0.5 \le l \le 1.5 \\ 0, & \text{otherwise} \end{cases} \\ f_P(l) &= e^{10\cdot l - 15} \\ f_V(v) &== 1 \end{aligned} \tag{6}$$

Through the force–length curve fitting algorithm described in [21], and [22], q_0, q_1, q_2 are set to be constants: $q_0 = -2.12$, $q_1 = 6.09$, and $q_2 = -3.20$.

The musculotendon length l^{mt} can be described as follows:

$$l^{mt} = l^t + l^m \cdot \cos(\phi) \tag{7}$$

where l^t is the length of the tendon.

The simplifications of F_0^m, l^t, l_0^m, ϕ can also replace the biomechanical parameters [23], [24]. The musculotendon length l^{mt} can be simplified by a polynomial and described as a first-order polynomial [25], [26]:

$$l^{mt} = b_0 + b_1 \cdot \theta \tag{8}$$

where θ is the joint angle, b_0 and b_1 are constants. Then, we get the moment arm r as follows:

$$r = \frac{\partial l^{mt}(\theta)}{\partial \theta} = b_1 \tag{9}$$

Then the joint moment τ can be described as follows:

$$\tau = F^{mt} \cdot r \tag{10}$$

2) EMG–Driven Joint Motion Model: The angular acceleration is described as follows:

$$\ddot{\theta} = \frac{1}{I_e} \cdot (\tau - \tau_{eg}), \quad \tau_{eg} = \tau_{egm} \cdot \sin(\theta) \tag{11}$$

where I_e is the moment of inertia, which can be assumed as constant for fixed load, τ_{eg} is the gravity torque, and τ_{egm} is the maximum of τ_{eg}.

By combining the equations above, the angular acceleration $\ddot{\theta}$ can be described as follows:

$$\ddot{\theta} = (s_0 + s_1 \cdot \theta + s_2 \cdot \theta^2) \cdot a(k) + s_3 \cdot e^{s_4 \cdot \theta} - s_5 \cdot \sin(\theta) \tag{12}$$

where $s_i (i = 0, 1, \ldots, 5)$ are constants computed as follows:

$$\begin{cases} s_0 = \dfrac{k_0 \cdot F_0^m \cdot b_1 \cdot \cos\phi}{I_e} + \dfrac{k_1 \cdot F_0^m \cdot (b_0 - l^t) \cdot b_1}{l_0^m \cdot I_e} \\ \quad + \dfrac{k_2 \cdot F_0^m \cdot (b_0 - l^t)^2 \cdot b_1}{(l_0^m)^2 \cdot I_e \cdot \cos\phi} \\ s_1 = \dfrac{k_1 \cdot F_0^m \cdot (b_1)^2}{l_0^m \cdot I_e} + \dfrac{2 \cdot k_2 \cdot (b_0 - l^t) \cdot (b_1)^2}{(l_0^m)^2 \cdot I_e \cdot \cos\phi} \\ s_2 = \dfrac{k_2 \cdot F_0^m \cdot (b_1)^3}{(l_0^m)^2 \cdot I_e \cdot \cos\phi} \\ s_3 = \dfrac{F_0^m \cdot b_1 \cdot \cos\phi}{I_e} \cdot \exp\left(\dfrac{10 \cdot (b_0 - l^t) \cdot (b_1)^2}{l_0^m \cdot \cos\phi} - 15\right) \\ s_4 = \dfrac{10 \cdot b_1}{l_0^m \cdot \cos\phi}, s_5 = \dfrac{\tau_{egm}}{I_e} \end{cases} \tag{13}$$

Then, we obtain the joint motion model in discrete time as follows:

$$\begin{cases} \ddot{\theta}_{k+1} = (s_0 + s_1 \cdot \theta_k + s_2 \cdot \theta_k^2) \cdot a(k) + s_3 \cdot e^{s_4 \theta_k} - s_5 \cdot \sin(\theta_k) \\ \dot{\theta}_{k+1} = \dot{\theta}_k + \ddot{\theta}_k \cdot T_s \\ \theta_{k+1} = \theta_k + \dot{\theta}_k \cdot T_s \end{cases} \tag{14}$$

where T_s is the sampling time, $\dot{\theta}_k$ is the joint angular velocity, and θ_k is the joint position.

3) EMG Features and State-Space Model: The simplified EMG-driven joint motion model involves two problems. First, the model omits certain physiological parameters. Second, the biomechanical parameters are variable in virtue of different conditions of the body state. These problems cause accumulative errors in the recursive calculation of the joint angle. To eliminate the accumulative errors, we put forward a measure equation providing the joint angle measurements as feedback, which then lead to a sEMG state-space model. We built the measure equation by RMS and WC in this study.

$$X_{rms} = \sqrt{\frac{1}{N-1} \sum_{i=0}^{N-1} x_i^2} \tag{15}$$

$$N = T_{win} / T_{emg} \tag{16}$$

where X_{rms} is RMS, x_i^2 is the data sequences, N is the size of a time window, T_{win} is the time window length, and T_{emg} is the sampling period of sEMG.

WC was extracted by discrete wavelet transform:

$$\begin{aligned} f(t) &= A_J + \sum\nolimits_{j \le J} D_j \\ A_J &= \sum\nolimits_{j > J} D_j \\ D_j &= \sum\nolimits_{k \in Z} \alpha_{j,k} \phi_{j,t}(t) \end{aligned} \tag{17}$$

where $f(t)$ is the sEMG signals at level j, Z is the positive integer, $\alpha_{j,k}$ is WC, and $\phi_{j,t}(t)$ is a mother wavelet function.

The sEMG signal $x(n) = CD1 + CD2 + CD3 + CD4 + CA4$ was decomposed to four layers by the db3 wavelet, then the absolute value of $CA4$ is regarded as the WC feature of sEMG signal.

To relate sEMG features with the joint motion, the following second-order polynomial was used as the fitting function:

$$y_k^u = c_0^u + c_1^u \cdot \dot{\theta}_k + c_2^u \cdot \theta_k + c_3^u \cdot \dot{\theta}_k^2 + c_4^u \cdot \theta_k^2 + c_5^u \cdot \dot{\theta}_k \cdot \theta_k \tag{18}$$

where $u = 1,2$; $c_i^u (i = 0, 1, \ldots, 5)$ are constant parameters. y_k^1 and y_k^2 represent the RMS and WC at time k.

By combining the equations above, the nonlinear expression of the model was obtained:

$$\begin{cases} x_{k+1} = f(x_k, a_k) + \omega_k \\ y_{k+1} = h(x_{k+1}) + \upsilon_{k+1} \end{cases} \tag{19}$$

$$f(x_k, a_k) = \begin{bmatrix} (s_0 + s_1 \cdot \theta_k + s_2 \cdot \theta_k^2) \cdot a_k + s_3 \cdot e^{s_4 \cdot \theta_k} - s_5 \cdot \sin(\theta_k) \\ \dot{\theta}_k + \ddot{\theta}_k \cdot T \\ \theta_k + \dot{\theta}_k \cdot T \end{bmatrix} \tag{20}$$

$$h(x_k) = \begin{bmatrix} c_0^1 + c_1^1 \cdot \dot{\theta}_k + c_2^1 \cdot \theta_k + c_3^1 \cdot \dot{\theta}_k^2 + c_4^1 \cdot \theta_k^2 + c_5^1 \cdot \dot{\theta}_k \cdot \theta_k \\ c_0^2 + c_1^2 \cdot \dot{\theta}_k + c_2^2 \cdot \theta_k + c_3^2 \cdot \dot{\theta}_k^2 + c_4^2 \cdot \theta_k^2 + c_5^2 \cdot \dot{\theta}_k \cdot \theta_k \end{bmatrix} \tag{21}$$

where $x_k = [\ddot{\theta}_k \dot{\theta}_k \ \theta_k]^T$, $y_k = [y_k^1 y_k^2]^T$, $a_k = a(k)$, ω_k is the process noise, and υ_k is the measurement noise.

4) The Interference Rejection of External Load: Because the muscle activation, RMS, and WC are all influenced by the external loads, we used an interference rejection algorithm of external load (IRL) to solve the problem:

$$\psi(m) = \lambda_0 + \lambda_1 \cdot m + \lambda_2 \cdot m^2 \tag{22}$$

where $\psi(m)$ is the relationship between external load m and the maximum value of EMG state, which includes EMG signal $e(k)$, RMS, and WC, $\lambda_i (i = 0, 1, 2, 3)$ are constant coefficients to be calculated [27].

Then, we get the normalized features:

$$\mathrm{RMS}^n = \frac{RMS}{\psi_{RMS}(m)}, \quad \mathrm{WC}^n = \frac{WC}{\psi_{WC}(m)} \tag{23}$$

where $\psi_{RMS}(m)$ and $\psi_{WC}(m)$ are RMS and WC at the external load m, respectively.

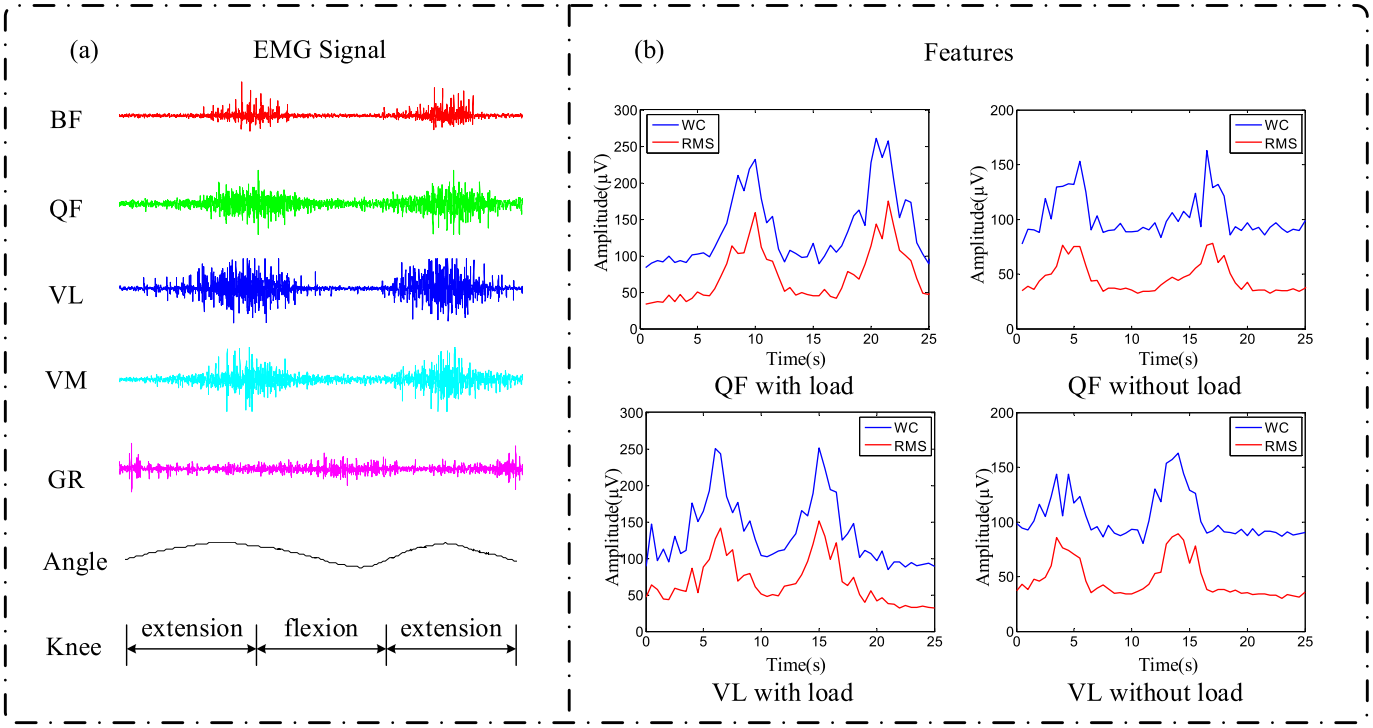

Fig. 4. (a) Raw sEMG signal of BF, QF, VL, VM, GR and angle signal of knee-joint motion. (b) the RMS and WC features of QF with load, QF without load, VL with load and VL without load.

5) Unscented Particle Filter: Based on the proposed motion model, we used the unscented Kalman filter (UKF) to estimate the joint motion [28]. The UKF extracts $2n_x+1$ sigma points from the Gaussian and passes these through the nonlinear state and measurement functions. The UKF can be summarized as follows:

Calculate the sigma points:

$$\begin{aligned} X_0 &= \bar{x},\ X_i = \bar{x} + (\sqrt{(n_x+\lambda)P_x})_i \quad (i{=}1,\ldots,n_x) \\ X_i &= \bar{x} - (\sqrt{(n_x+\lambda)P_x})_i \quad (i = n_x,\ldots,2n_x) \\ W_0^{(m)} &= \frac{\lambda}{(n_x+\lambda)}, \quad W_0^{(c)} = W_0^{(m)} + (1-\alpha^2+\beta) \\ W_i^{(m)} &= \frac{1}{2\cdot(n+\lambda)}, \quad \lambda = \alpha^2(n_x+\kappa) - n_x \end{aligned} \tag{24}$$

where n_x is the dimension of x; $\bar{x}$ and P_x are the mean and covariance of x, respectively; κ is the scaling parameter; and α, β are the control parameters.

Sigma points:

$$X_{t-1}^a = [\bar{x}_{t-1}^a \bar{x}_{t-1}^a \pm \sqrt{(n_a+\lambda)P_{t-1}^a}] \tag{25}$$

Time update:

$$\begin{aligned} X_{t|t-1}^x &= f(X_{t-1}^x, X_{t-1}^v),\ \bar{x}_{t|t-1} = \sum_{i=0}^{2n_a} W_i^{(m)} X_{i,t|t-1}^x \\ Y_{t|t-1} &= h(X_{t-1}^x, X_{t-1}^n),\ \bar{y}_{t|t-1} = \sum_{i=0}^{2n_a} W_i^{(m)} Y_{i,t|t-1}^x \\ P_{t|t-1} &= \sum_{i=0}^{2n_a} W_i^{(c)} [X_{i,t|t-1}^x - \bar{x}_{t|t-1}][X_{i,t|t-1}^x - \bar{x}_{t|t-1}]^T \end{aligned} \tag{26}$$

where $Y_i = g(X_i)$ and $y = g(x)$ is a non-linear transformation.

Measurement update:

$$\begin{aligned} P_{y_t y_t} &= \sum_{i=0}^{2n_a} W_i^{(c)} [Y_{i,t|t-1} - \bar{y}_{t|t-1}][Y_{i,t|t-1} - \bar{y}_{t|t-1}]^T \\ P_{x_t y_t} &= \sum_{i=0}^{2n_a} W_i^{(c)} [X_{i,t|t-1}^x - \bar{x}_{t|t-1}][Y_{i,t|t-1}^x - \bar{y}_{t|t-1}]^T, \\ K_t &= P_{x_t y_t} P_{y_t y_t}^{-1} \\ \bar{x}_t &= \bar{x}_{t|t-1} + K_t(y_t - \bar{y}_{t|t-1}),\ P_t = P_{t|t-1} - K_t P_{y_t y_t} K_t^T \end{aligned} \tag{27}$$

III. Experimental Results

Ten subjects were conducted with two different situations, with load (3kg) and without load. Each subject completed the action of knee joint flexion-extension, ankle joint flexion-extension, and simultaneous motion in 10s, and repeated four times. The feature dataset of the joint movement was input into the proposed model. Five-fold cross validation was used to perform the simulation.

Fig. 4 and Fig. 5 show the sEMG signals, joint angle, and features of knee-joint and ankle-joint motions recorded from a typical subject. The parameters which were identified offline are list in Table I and II. Table I shows the identified values concerning external loads. Table II shows the coefficients of fitted polynomials for IRL.

Fig. 6 shows that both estimations based on HMM diverged after seconds. For ankle, the angle cannot be estimated after 15s. And for knee, the angle cannot be estimated after 6.5s.

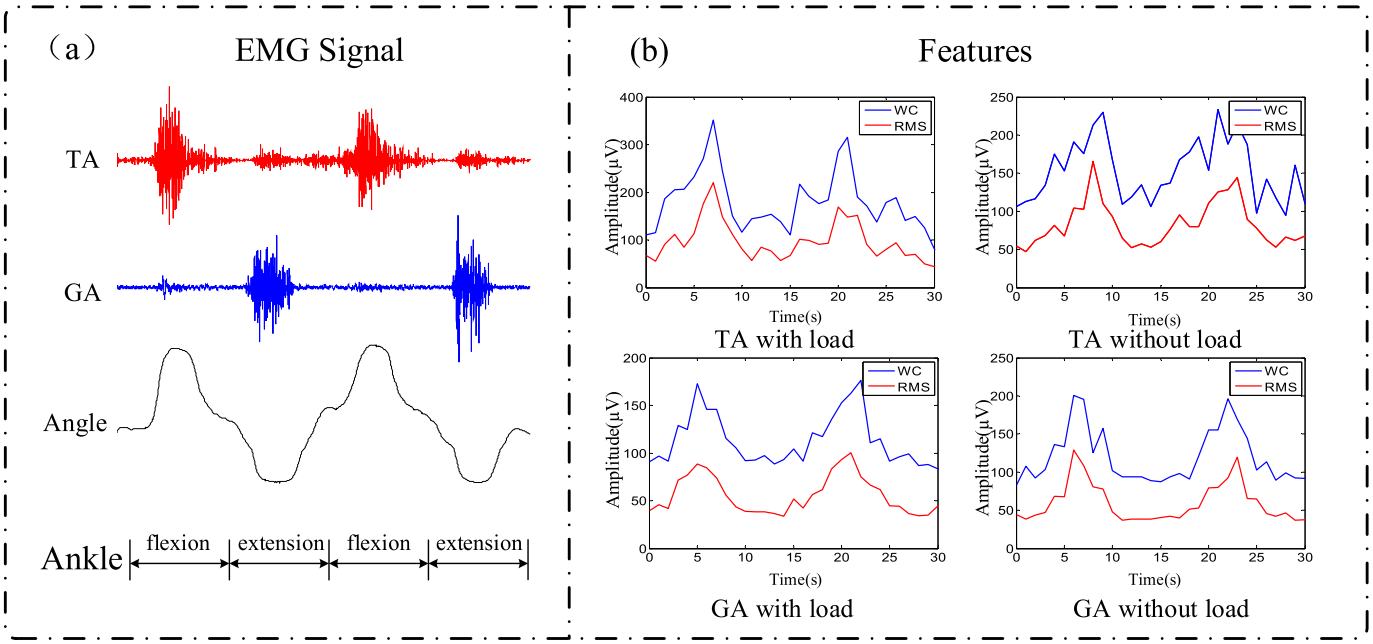

Fig. 5. (a) Raw sEMG signal of TA, GA and angle signal of ankle-joint motion. (b) the RMS and WC features of TA with load, TA without load, GA with load and GA without load.

TABLE I
IDENTIFIED PARAMETERS WITH LOAD AND WITHOUT LOAD

s_i	s_0	s_1	s_2	s_3	s_4	s_5
With load	5.26	-8.57	-5.37	0.02	-0.13	0.58
Without load	1.88	-1.97	-0.56	0.08	-0.68	0.24

c_i^1	c_0^1	c_1^1	c_2^1	c_3^1	c_4^1	c_5^1
With load	-2.67	-0.07	4.43	-0.24	-1.59	0.02
Without load	-0.39	0.01	1.57	0.12	-0.29	0.24

c_i^2	c_0^2	c_1^2	c_2^2	c_3^2	c_4^2	c_5^2
With load	-6.43	0.22	8.35	0.03	-2.54	-0.04
Without load	-2.34	0.23	8.69	0.48	-2.41	-0.15

TABLE II
COEFFICIENTS OF THE FITTING POLYNOMIALS FOR IRL

	λ_0	λ_1	λ_2
ψ_{RMS}	0.6877	2.1863	-0.9386
ψ_{WC}	1.6553	8.6489	-2.4643

However, this would not be the case with proposed model. The sEMG state-space model overcame the error accumulation, while improving the estimation accuracy significantly.

To verify the improvement of the load and IRL, we used the sEMG state-space model to perform the UKF without load and IRL, and then did the same experiment with load and IRL. Fig. 7 shows the estimation results of knee-joint and ankle-joint angles.

Also, we used the proposed model to estimate the joint angles of simultaneous joint motion. Fig. 8 shows the experimental results of the estimated simultaneous motion angles.

From Fig. 7 and 8, we can see that the model with load and IRL has better estimation results than that without load and IRL in both individual joint motion and simultaneous joint motion. The reason is that the amplitude of EMG will increase with the load. Then the features extracted from the EMG signals will be more obvious and IRL can rejection the interference of external load, which can improve the estimation accuracy.

The root–mean–square error (RMSE) and the correlation coefficient (CC) were used to represent the angle-estimation accuracy. Fig. 9 shows the mean RMSE of ten subjects for simultaneous joint motion in the sections of with load or without load, with IRL or without IRL. The performance

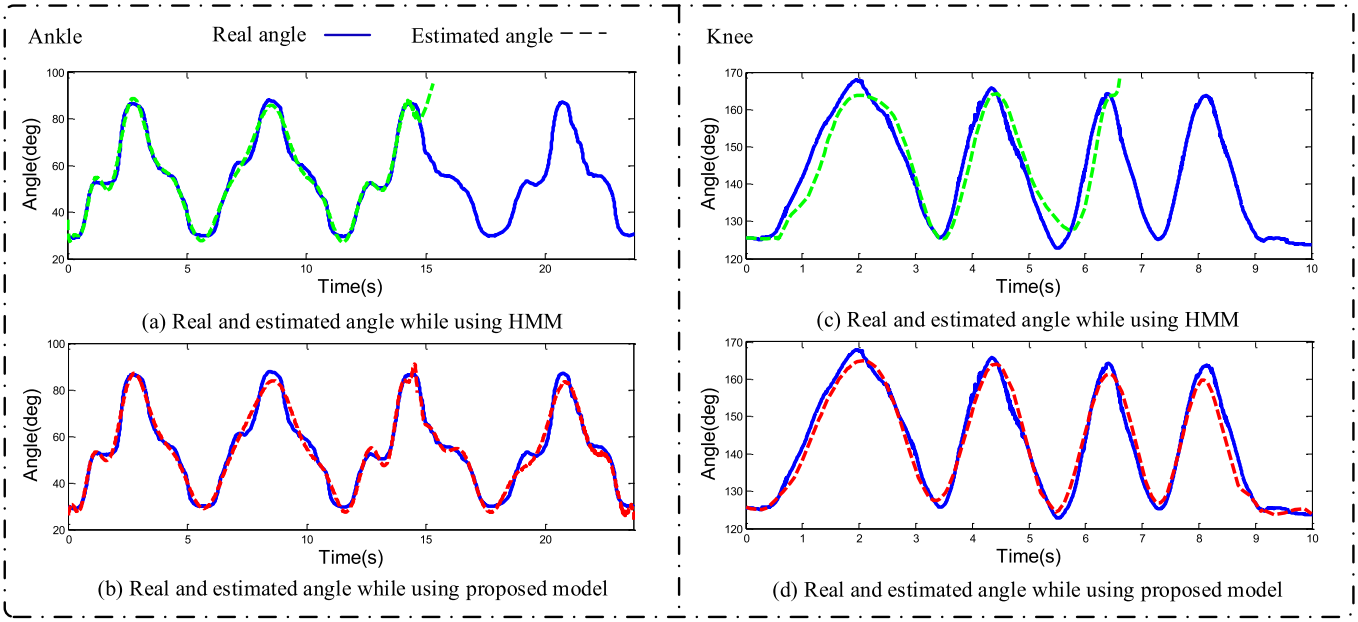

Fig. 6. Real and estimated angle while using HMM and proposed model. (blue) Codamition measurement. (green) Estimated value while using HMM. (red) Estimated value while using the proposed model.

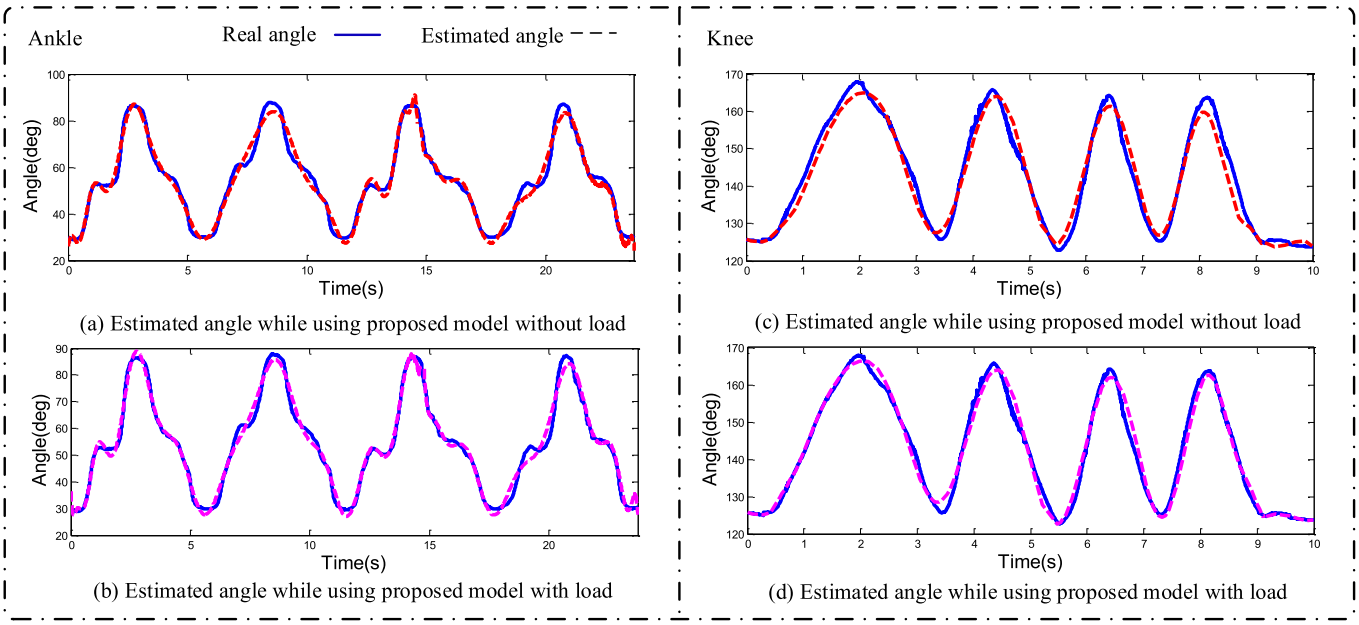

Fig. 7. (a) The estimation results of ankle-joint motion without load and IRL. (b) The estimation results of ankle-joint motion with load and IRL. (c) The estimation results of knee-joint motion without load and IRL. (d) The estimation results of knee-joint motion with load and IRL. (blue) Codamition measurement. (red) Without load and IRL. (purple) With load and IRL.

evaluation of the models with load and IRL and without load and IRL are shown in Table III.

From Fig. 9 and Table III, we can see that the load and IRL can improve the estimation accuracy significantly. And the mean RMSE for knee-joint motion, ankle-joint motion, and simultaneous motion of the proposed model are 5.1143°±0.4217°, 5.2647°±0.4963°, and 6.3941°±0.6173°, respectively, which indicates that the estimation results of individual joint motion are better than that of simultaneous motion. The reason is that a muscle can control different joint motions and the influence of simultaneous joint motion on relevant muscles is more complicated than that of individual joint motion.

For comparison, five representative classification techniques, backpropagation neural network (BPNN)[29], generalized regression neural network (GRNN) [30], fuzzy min-max neural network (FMMNN) [31], GFWSVM [12] and nonlinear auto regressive with exogenous inputs structure based multiple layer perceptron neural network model (NARX-MLPNN) [32] were considered and shown in Table IV.

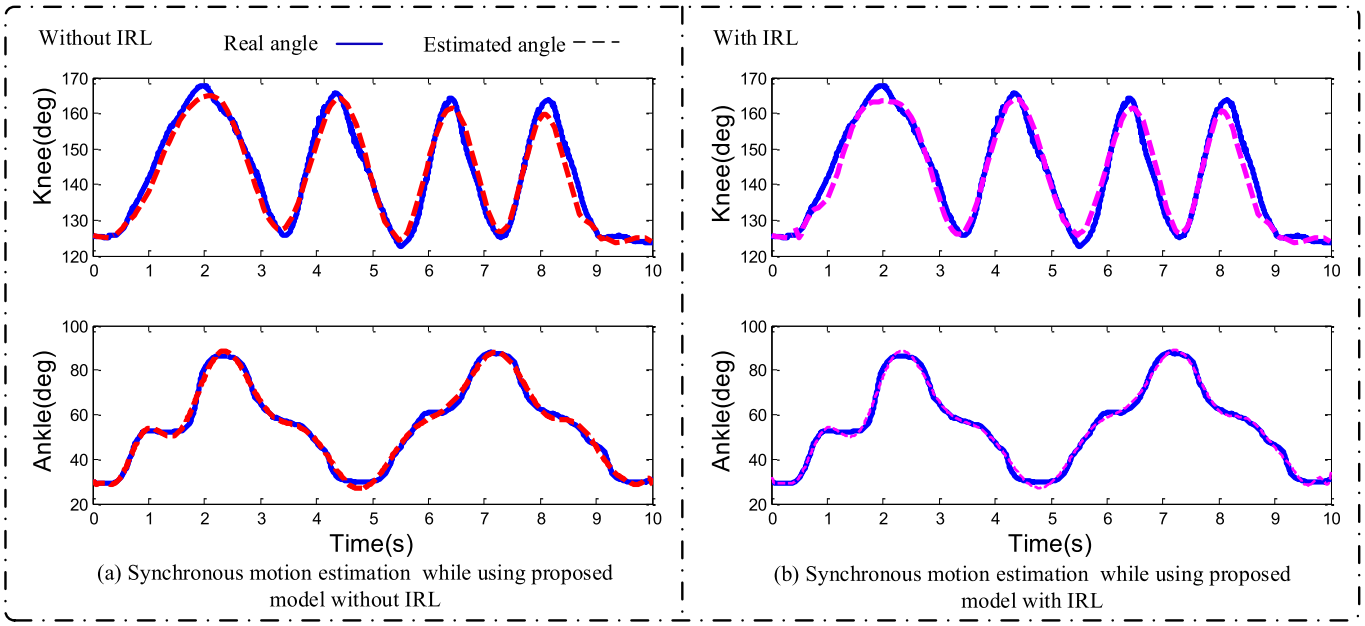

Fig. 8. (a) The estimation results of simultaneous motion without load and IRL. (b) The estimation results of simultaneous motion with load and IRL. (blue) Codamition measurement. (red) Without load and IRL. (purple) With load and IRL.

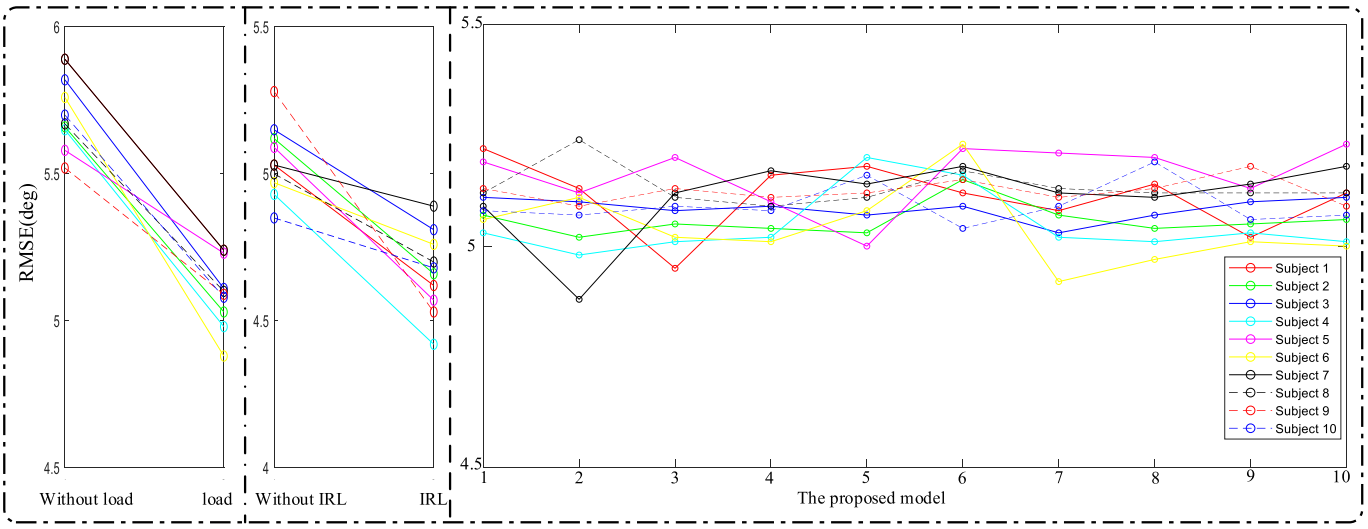

Fig. 9. The mean RMSE of ten subjects for simultaneous joint motion in the sections of with load or without load, with IRL or without IRL. Ten colored lines denote the accuracies of ten subjects. The numbers 1-10 denote the different datasets.

Table IV shows that the mean RMSE and CC for knee-joint motion, ankle-joint motion, and simultaneous motion of the proposed model are 5.1143° and 0.9531, 5.2647° and 0.9617, 6.3941° and 0.9513, respectively. The estimated effect of BPNN is worst. Compared with NARX-MLPNN, the mean RMSE of ankle-joint motion, and simultaneous motion of the proposed model is smaller. Meanwhile, the mean RMSE values of the two models differ little for knee-joint motion. In conclusion, the estimation accuracy of the EMG state-space model is better than other estimation methods.

IV. Discussion

Simultaneous and continuous joint angle estimation plays an important role in motion intention recognition and rehabilitation training. The research of simultaneous and continuous joint angle is more valuable in the natural and stable control of powered prosthesis, exoskeletons and rehabilitative robots, compared with motion classification.

The purpose of this study is to build a sEMG state-space model to estimate continuous joint movements from sEMG signals. Here are some problems in the simplified EMG-driven joint motion model: First, the model omits certain physiological parameters. Second, the biomechanical parameters are variable in virtue of different conditions of the body state. These problems cause accumulative errors in the recursive calculation of the joint angle. Therefore, we used a measure equation providing the joint angle measurements as feedback, then lead to the model. Since the muscle activation, the feature extracted are all influenced by the external loads, an interference rejection algorithm of IRL is used to solve the problem.

TABLE III
THE EVALUATION FOR THE PERFORMANCES OF THE PROPOSED MODELS (RMSE, CC)

Joint Motion		Knee		Ankle		Knee-Ankle	
		RMSE	CC	RMSE	CC	RMSE	CC
HMM	without load	14.1334± 2.3432	0.7868± 0.0637	13.8301± 1.8253	0.7929± 0.0657	15.4831± 2.7485	0.7632± 0.0673
	load	13.4357± 2.1743	0.7941± 0.0683	13.5294± 1.7496	0.7862± 0.0612	14.5179± 2.4523	0.7891± 0.0726
Proposed Model	without load	5.4981± 0.4325	0.9592± 0.0362	6.1348± 0.5174	0.9513± 0.0382	7.1769± 0.6351	0.9444± 0.0416
	load	5.1143± 0.4217	0.9531± 0.0376	5.2647± 0.4963	0.9617± 0.0384	6.3941± 0.6173	0.9513± 0.0437
	load and IRL	4.8492± 0.3864	0.9617± 0.0395	4.5142± 0.3333	0.9691± 0.0373	6.1917± 0.5972	0.9576± 0.0417

TABLE IV
COMPARISONS AMONG PROPOSED MODEL AND OTHER CLASSIFICATION (RMSE, CC)

Joint Motion		Knee		Ankle		Knee-Ankle	
		RMSE	CC	RMSE	CC	RMSE	CC
BPNN	without load	9.1354± 1.8732	0.9219± 0.0474	9.1179± 1.8463	0.9293± 0.0436	9.9335± 1.9351	0.9137± 0.0542
	load and IRL	8.7649± 1.7461	0.9204± 0.0453	8.6489± 1.6492	0.9296± 0.0423	9.2486± 1.9162	0.9035± 0.0563
GRNN	without load	8.5196± 1.7324	0.9281± 0.0451	8.3491± 1.6952	0.9249± 0.0463	8.7648± 1.7532	0.9269± 0.0471
	load and IRL	7.9317± 1.6932	0.9217± 0.0424	7.6848± 1.6731	0.9397± 0.0482	8.4973± 1.7691	0.9219± 0.0465
FMMNN	without load	7.1354± 1.2693	0.9402± 0.0431	9.1179± 1.9257	0.9303± 0.0462	9.1946± 2.1575	0.9247± 0.0472
	load and IRL	6.7649± 1.0351	0.9414± 0.0416	8.6489± 1.7462	0.9416± 0.0431	8.9264± 1.9734	0.9349± 0.0451
GFWSVM	without load	6.4763± 0.8237	0.9563± 0.0385	6.5594± 0.9421	0.9543± 0.0403	7.8432± 1.5341	0.9513± 0.0394
	load and IRL	5.9364± 0.6174	0.9554± 0.0372	6.1526± 0.8263	0.9538± 0.0383	7.2581± 1.4637	0.9531± 0.0387
NARX-MLP NN	without load	5.2153± 0.4653	0.9561± 0.0375	6.2536± 0.5435	0.9553± 0.0415	8.3465± 1.7364	0.9472± 0.0436
	load and IRL	4.7932± 0.4384	0.9653± 0.0382	5.8741± 0.4637	0.9526± 0.0392	7.7492± 1.4276	0.9532± 0.0415
Proposed Model	without load	5.4981± 0.4325	0.9592± 0.0362	6.1348± 0.5174	0.9513± 0.0382	7.1769± 0.6351	0.9444± 0.0416
	load and IRL	4.8492± 0.3864	0.9617± 0.0395	4.5142± 0.3333	0.9691± 0.0373	6.1917± 0.5972	0.9576± 0.0425

The results show that the proposed model improved the estimation accuracy of knee-joint motion, ankle-joint motion, and knee-ankle simultaneous motion. The mean RMSE of individual joint motion and simultaneous motion is less than 5.3° and 6.4°, which also indicates that the sEMG state-space model has high estimation accuracy. Moreover, compared with the conventional regression methods, the proposed model exhibits the best performance in the experiments.

However, there are several important limitations related to this study that need further development to be used in rehabilitation medical robots under real-world conditions. This study collected sEMG and joint angle signals with specific motions from healthy subjects. It is not known how well this model would work in a real scenario with unscripted free-form activities performed by elderly or real patients. Although, there is no considerable difference in the characteristics of sEMG between subjects with disabilities and without disabilities, the amplitude and frequency of the signal will still influence the estimation accuracy. These conditions need to be investigated before using the proposed sEMG state-space model for clinical purposes.

V. CONCLUSION

We integrated forward dynamics into HMM, and employed sEMG features (RMS, WC) to construct measure equations, and consequently formed a sEMG state-space model

to estimate continuous angle of knee-joint and ankle-joint. A normalization algorithm named IRL was used to reject the errors of angle estimation with load. Compared with traditional methods for angle estimation, the proposed model was shown to improve the estimation accuracy. In the future, the proposed sEMG state-space model will be utilized to estimate the simultaneous and continuous motions of multiple joints by the sEMG signals and can be applied to rehabilitation robots and exoskeleton robots.

REFERENCES

[1] J. L. Pons, *Wearable Robots: Biomechatronic Exoskeletons*. Hoboken, NJ, USA: Wiley, 2008.

[2] Y. Hu, Z. Li, G. Li, P. Yuan, C. Yang, and R. Song, "Development of sensory-motor fusion-based manipulation and grasping control for a robotic hand-eye system," *IEEE Trans. Syst., Man, Cybern. Syst.*, vol. 47, no. 7, pp. 1169–1180, Jul. 2017.

[3] A. Cutti, P. Perego, M. Fusca, R. Sacchetti, and G. Andreoni, "Assessment of lower limb prosthesis through wearable sensors and thermography," *Sensors*, vol. 14, no. 3, pp. 5041–5055, Mar. 2014.

[4] J. Qi, G. Jiang, G. Li, Y. Sun, and B. Tao, "Surface EMG hand gesture recognition system based on PCA and GRNN," *Neural Comput. Appl.*, vol. 32, pp. 6343–6351, Mar. 2019.

[5] J. Liu and P. Zhou, "A novel myoelectric pattern recognition strategy for hand function restoration after incomplete cervical spinal cord injury," *IEEE Trans. Neural Syst. Rehabil. Eng.*, vol. 21, no. 1, pp. 96–103, Jan. 2013.

[6] X. Zhang, X. Chen, Y. Li, V. Lantz, K. Wang, and J. Yang, "A framework for hand gesture recognition based on accelerometer and EMG sensors," *IEEE Trans. Syst., Man, Cybern., A, Syst. Humans*, vol. 41, no. 6, pp. 1064–1076, Nov. 2011.

[7] B. Cesqui, P. Tropea, S. Micera, and H. Krebs, "EMG-based pattern recognition approach in post stroke robot-aided rehabilitation: A feasibility study," *J. Neuroeng. Rehabil.*, vol. 10, no. 1, p. 75, 2013.

[8] Y. M. Aung and A. Al-Jumaily, "Estimation of upper limb joint angle using surface EMG signal," *Int. J. Adv. Robotic Syst.*, vol. 10, no. 10, p. 369, Oct. 2013.

[9] C. Huihui, G. Farong, C. Chao, and T. Taixing, "Estimation of ankle angle based on multi-feature fusion with random forest," in *Proc. 37th Chin. Control Conf. (CCC)*, Wuhan, China, Jul. 2018, pp. 5549–5553.

[10] Y. Chen *et al.*, "A continuous estimation model of upper limb joint angles by using surface electromyography and deep learning method," *IEEE Access*, vol. 7, pp. 174940–174950, 2019.

[11] Z. Li, C. Xu, Q. Wei, C. Shi, and C.-Y. Su, "Human-inspired control of dual-arm exoskeleton robots with force and impedance adaptation," *IEEE Trans. Syst., Man, Cybern. Syst.*, vol. 50, no. 12, pp. 5296–5305, Dec. 2020.

[12] F. Xiao, Y. Wang, Y. Gao, Y. Zhu, and J. Zhao, "Continuous estimation of elbow joint angle by multiple features of surface electromyographic using grey features weighted support vector machine," *J. Med. Imag. Health Informat.*, vol. 7, no. 3, pp. 574–583, Jun. 2017.

[13] D. Blana, J. G. Hincapie, E. K. Chadwick, and R. F. Kirsch, "A musculoskeletal model of the upper extremity for use in the development of neuroprosthetic systems," *J. Biomech.*, vol. 41, no. 8, pp. 1714–1721, 2008.

[14] M. Sartori, D. G. Llyod, and D. Farina, "Neural data-driven musculoskeletal modeling for personalized neurorehabilitation technologies," *IEEE Trans. Biomed. Eng.*, vol. 63, no. 5, pp. 879–893, May 2016.

[15] M. Sartori, G. Durandau, S. Došen, and D. Farina, "Robust simultaneous myoelectric control of multiple degrees of freedom in wrist-hand prostheses by real-time neuromusculoskeletal modeling," *J. Neural Eng.*, vol. 15, no. 6, Dec. 2018, Art. no. 066026.

[16] T. S. Buchanan, D. G. Lloyd, K. Manal, and T. F. Besier, "Neuromusculoskeletal modeling: Estimation of muscle forces and joint moments and movements from measurements of neural command," *J. Appl. Biomech.*, vol. 20, no. 4, pp. 367–395, Nov. 2004.

[17] C. Fleischer and G. Hommel, "A human-exoskeleton interface utilizing electromyography," *IEEE Trans. Robot.*, vol. 24, no. 4, pp. 872–882, Aug. 2008.

[18] N. A. Shrirao, N. P. Reddy, and D. R. Kosuri, "Neural network committees for finger joint angle estimation from surface EMG signals," *Biomed. Eng. OnLine*, vol. 8, no. 1, p. 2, 2009.

[19] Q. Shao, D. N. Bassett, K. Manal, and T. S. Buchanan, "An EMG-driven model to estimate muscle forces and joint moments in stroke patients," *Comput. Biol. Med.*, vol. 39, no. 12, pp. 1083–1088, Dec. 2009.

[20] D. G. Lloyd and T. F. Besier, "An EMG-driven musculoskeletal model to estimate muscle forces and knee joint moments *in vivo*," *J. Biomech.*, vol. 36, no. 6, pp. 765–776, Jun. 2003.

[21] R. D. Woittiez, P. A. Huijing, H. B. K. Boom, and R. H. Rozendal, "A three-dimensional muscle model: A quantified relation between form and function of skeletal muscles," *J. Morphol.*, vol. 182, no. 1, pp. 95–113, 1984.

[22] Q. C. Ding, A. B. Xiong, X. G. Zhao, and J. D. Han, "A novel EMG-driven state space model for the estimation of continuous joint movements," in *Proc. IEEE Int. Conf. Syst., Man, Cybern.*, Oct. 2011, pp. 2891–2897.

[23] F. E. Zajac, "Muscle and tendon: Properties, models, scaling, and application to biomechanics and motor control," *Crit. Rev. Biomed. Eng.*, vol. 17, no. 4, pp. 359–411, 1989.

[24] K. R. S. Holzbaur, W. M. Murray, and S. L. Delp, "A model of the upper extremity for simulating musculoskeletal surgery and analyzing neuromuscular control," *Ann. Biomed. Eng.*, vol. 33, no. 6, pp. 829–840, Jun. 2005.

[25] P. Pigeon, L. Yahia, and A. G. Feldman, "Moment arms and lengths of human upper limb muscles as functions of joint angles," *J. Biomech.*, vol. 29, no. 10, pp. 1365–1370, Oct. 1996.

[26] J. W. Ramsay, B. V. Hunter, and R. V. Gonzalez, "Muscle moment arm and normalized moment contributions as reference data for musculoskeletal elbow and wrist joint models," *J. Biomech.*, vol. 42, no. 4, pp. 463–473, Mar. 2009.

[27] J. Han, Q. Ding, A. Xiong, and X. Zhao, "A state-space EMG model for the estimation of continuous joint movements," *IEEE Trans. Ind. Electron.*, vol. 62, no. 7, pp. 4267–4275, Jul. 2015.

[28] S. J. Julier and J. K. Uhlmann, "New extension of the Kalman filter to nonlinear systems," *Proc. SPIE*, vol. 3068, pp. 182–193, Jul. 1997.

[29] P. D. Heermann and N. Khazenie, "Classification of multispectral remote sensing data using a back-propagation neural network," *IEEE Trans. Geosci. Remote Sens.*, vol. 30, no. 1, pp. 81–88, Jan. 1992.

[30] D. F. Specht, "A general regression neural network," *IEEE Trans. Neural Netw.*, vol. 2, no. 6, pp. 568–576, Nov. 1991.

[31] M. F. Mohammed, C. P. Lim, and A. Quteishat, "A novel trust measurement method based on certified belief in strength for a multi-agent classifier system," *Neural Comput. Appl.*, vol. 24, no. 2, pp. 421–429, Feb. 2014.

[32] R. Raj and K. S. Sivanandan, "Elbow joint angle and elbow movement velocity estimation using NARX-multiple layer perceptron neural network model with surface EMG time domain parameters," *J. Back Musculoskeletal Rehabil.*, vol. 30, no. 3, pp. 515–525, May 2017.

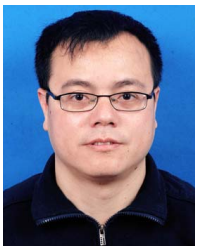

Xugang Xi received the B.S., M.S., and Ph.D. degrees from Hangzhou Dianzi University, Hangzhou, China. He is currently a Professor with Hangzhou Dianzi University. His research interests include biomedical signal processing, human–robot interaction, and rehabilitation robot.

Wenjun Jiang received the B.S. degree from Hangzhou Dianzi University in 2018, where he is currently pursuing the master's degree. His research interests include biomedical signal processing and rehabilitation robot.

Xian Hua received the M.S. degree from Zhejiang Chinese Medical University in 2012. She is currently a Clinician with the Jinhua People's Hospital. Her current research interests include electroencephalograph and application of artificial intelligence in medical field.

Huijiao Wang received the B.Sc. degree in mechatronics engineering in 1997, the M.Sc. degree in control theory and control engineering from Hangzhou Dianzi University, Hangzhou, China, in 2003, and the Ph.D. degree in control science and engineering from Zhejiang University, Hangzhou, in 2008. From November 2013 to October 2014, she was an Academic Visitor with the School of Electrical and Electronic Engineering, The University of Adelaide, Adelaide, SA, Australia. She is currently a Professor with the Fair Friend Institute of Electromechanics, Hangzhou Vocational and Technical College. Her current research interests include event-triggered control, intelligent control, and networked control systems.

Chen Yang received the master's degree from Hangzhou Dianzi University in 2020. His research interests include biomedical signal processing and rehabilitation robot.

Yun-Bo Zhao (Senior Member, IEEE) received the B.Sc. degree in mathematics from Shandong University, Jinan, China, in 2003, the M.Sc. degree in systems sciences from the Key Laboratory of Systems and Control, Chinese Academy of Sciences, Beijing, China, in 2007, and the Ph.D. degree in control engineering from the University of South Wales (formerly University of Glamorgan), Pontypridd, U.K., in 2008. He has held a postdoctoral position with INRIA Grenoble, France; the University of Glasgow, U.K.; and the Imperial College London, U.K. He is currently a Professor with the Zhejiang University of Technology, Hangzhou, China. His research interests include networked control systems, systems biology, and artificial intelligence.

Seyed M. Miran received the Master of Science degree in statistics and the Ph.D. degree in systems engineering from the University of Akron, OH, USA. He is currently a Postdoctoral Fellow with the Biomedical Informatics Center, George Washington University, Washington, DC, USA. His current research interests include system design, applied probability and statistics, and multimodal human–computer interaction.

Zhizeng Luo received the Ph.D. degree from Zhejiang University in 1998. He is a Professor with Hangzhou Dianzi University. His current research interests include pattern recognition, biomedical engineering, and rehabilitation robot.